Multiple-Transmit Focusing for the Nondestructive Testing of Downhole Casings Based on Borehole Transient Electromagnetic Systems

CHANGZAN LIU[1], **BO DANG**[2], **HAIYAN WANG**[1], **(Member, IEEE),**
XIAOHONG SHEN[1], **(Member, IEEE), LING YANG**[2], **ZHIPING REN**[2], **(Member, IEEE),**
RUIRONG DANG[2], **YUZHU KANG**[1], **(Graduate Student Member, IEEE), AND BAOQUAN SUN**[3]

[1]School of Marine Science and Technology, Northwestern Polytechnical University, Xi'an 710072, China
[2]Shaanxi Key Laboratory of Measurement and Control Technology for Oil and Gas Wells, Xi'an Shiyou University, Xi'an 710065, China
[3]Petroleum Engineering Technology Research Institute, Shengli Oilfield Company, SINOPEC, Dongying 257000, China

Corresponding authors: Bo Dang (bodang521@126.com) and Haiyan Wang (hywang@nwpu.edu.cn)

ABSTRACT Borehole transient electromagnetic (TEM) array has proven to be efficient for the downhole nondestructive testing (NDT) of metal casings through the eddy-current property. However, restricted by bad downhole conditions, the simple increase of the receiving array is not sufficient enough for improving the downhole NDT performance. In this paper, we present a multiple-transmit focusing (MTF)-based borehole TEM system for the NDT of downhole casings. On the basis of the borehole TEM signal model, the response of the multiple-transmit array is derived by employing the matrix form of the borehole TEM response. It was shown that the excited magnetic field by the multiple-transmit array can be focused by weighting the current of each transmitter. Using this property, a modified linear constrained minimum variance-based multiple-transmitting array weighting method was proposed to realize the MTF. Moreover, a subarray partition approach was proposed to simplify the MTF realization, where the subarray weighting and mean square error were also analyzed. The MTF method performance was verified by applying it to a borehole TEM system for the NDTs of downhole casings. Finally, simulations and experiments were conducted, and the results demonstrated the effectiveness of the proposed method.

INDEX TERMS Borehole, transient electromagnetic, nondestructive testing, multiple-transmit focusing, linear constrained minimum variance.

I. INTRODUCTION

Owing to their significant feature of accessibility to targets, borehole measurements have been widely used in many research fields, such as mineral detection [1], [2], oil & gas exploration [3], [4], and geotechnical and environmental investigations [5]. In the field of the nondestructive testing (NDT) of downhole casings, a borehole transient electromagnetic (TEM) system enables highly accurate measurements using the transient (pulsed) properties of eddy-currents [6]–[8]. Unlike conventional pulsed eddy-current

NDT techniques, the design of eddy-current sensors as well as their signal processing for borehole measurements are strongly restricted by harsh environments, including narrow underground confined spaces [9], the large temperature range [10], and cumbrous metal tool housings against high wellbore pressure [11], which greatly affect the performance of borehole NDTs [12], [13].

A lot of research has been performed on the design and use of eddy-current sensors to improve the NDT performance of metal pipes. Considering the limited spaces for inner coil sensors, the multi-turn approach was proposed to enhance the eddy-current response as well as the signal-to-noise ratio (SNR), which are strongly reduced by high temperature and

The associate editor coordinating the review of this manuscript and approving it for publication was Xiaokang Yin.

metal tool housings [14]. To inspect the cracks of various shapes, a combination of longitudinal and transverse multi-turn sensors was introduced in [15], where the longitudinal sensors achieved better performance in detecting large areas, and the transverse sensors performed better in regards to the determination of crack shapes. The above kind of sensors was successfully applied to metal pipe inspections in the past several decades. However, the transmitting-receiving distance (TRD), which is also termed as the source distance, was ignored. In [16]–[18], the TRD effect was investigated using finite element analysis in a remote field pulsed eddy-current system. It was shown that the thickness of a metal pipe can be determined using the zero-crossing time method as well as through the phase shifting of the attenuated responses with respect to the TRD. In [19], using the correlation of multiple receivers with different TRDs, the TRD effect was employed to form a multi-receive single transmit borehole TEM system for the NDT of downhole casings. Furthermore, the multi-receive array was weighted according to the array signal processing in radar and sonar detection so as to improve the detection performance. These methods have been proven to be effective in the receiver design and signal processing, which are required for improving the NDT performance of downhole casings. Meanwhile, the NDT performance is also affected by excitation coils [20], [21].

At present, most of the research on excitation coils focuses on the design of single transmitters. Reference [22] analyzed the exciting frequency influence of eddy-current NDT on crack detection. In regards to the form of transverse probes, a rotating magnetic field excitation source with three-phase coils was presented in [23], where giant magneto-resistive sensors were employed as the receivers of an eddy-current system used for the NDT of metal pipes. Additionally, [24] presented a biorthogonal rectangular probe to improve the inspection resolution, and it was shown that the transmit magnetic field distribution is closely related to the shape and geometrical parameters of exciting coils. In [25], to simultaneously ensure better performance for both the detection range and longitudinal resolution, a small auxiliary probe was used to improve the resolution, and a large main probe was used to achieve a sufficient detection range in multi-pipe detection. However, the joint inversion of the data from two absolutely different probes was too complex to implement since the transmitter and receiver of the two probes were independent of each other. In contrast, in [26], a focusing transmitter was employed to cancel the direct coupling from the main transmitter so as to improve the detection performance in an open-hole induction logging system. Although the Doll's theory for the geometry factor correction [27], [28] may not be satisfied in a cased-hole with a high-conductivity metal casing, this method indicated an effective approach of the synthesized magnetic field focusing using a current-controlled coil array for improving the detection performance through the multiple transmitter technique.

In this study, inspired by the multi-coil array techniques with array weighting and magnetic field focusing,

a multiple-transmit focusing (MTF)-based borehole TEM array system for the NDT of downhole casings was proposed. Also, on the basis of the characteristics of the borehole TEM signal model, a modified linear constrained minimum variance (LCMV) criterion-based [29] multiple-transmitting array weighting method was proposed to realize magnetic focusing, and it was shown that the SNR can also be maximized using the MTF method. Moreover, to simplify the MTF realization, we also presented a novel transmitting array design method using a subarray partition approach. Finally, simulations and experiments were conducted, and the results demonstrated the effectiveness of the proposed method.

The rest of this paper is organized as follows. The borehole TEM signal model based on the multiple-transmitting array is presented in Section II. In Section III, the LCMV-based MTF method is presented for the multiple-transmitting array of borehole TEM systems, where the SNR performance of the proposed method is analyzed. The transmitting array design method using the subarray partition approach for the borehole TEM system is presented in Section IV. The experimental and simulation results are discussed in Section V. Finally, we concluded the paper in Section VI.

II. MULTIPLE-TRANSMITTING BOREHOLE TEM SYSTEM MODEL

Consider a multiple-transmitting borehole TEM array designed to consist of N symmetry transmitters with an inter-element spacing of $\Delta z = z_n - z_{n-1}$ and one receiver, where all of which are wound around a soft magnetic core in a cylindrically layered medium. The electrical and geometry parameters of the jth layer (μ_j, ε_j, σ_j, and r_j with $j = 1, 2, \ldots, J$) are illustrated in Fig. 1. We took the magnetic core to be the innermost layer. The receiver and the N transmitters are located in the second layer, with their number of turns denoted by N_R and N_T, respectively.
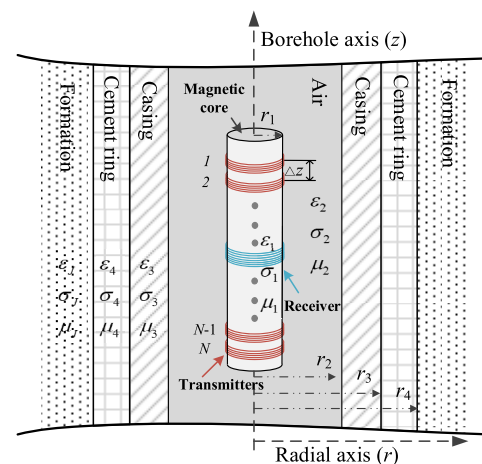

FIGURE 1. Multiple-transmitting borehole transient electromagnetic (TEM) system.

By solving the Helmholtz equations with the introduced variables x and λ, which satisfy $x^2 = \lambda^2 - \mu_1 \varepsilon_1 \omega^2 + i \mu_1 \sigma_1 \omega$, where ω denotes the angular frequency, and $-1 = i^2$,

the vertical component of the magnetic field at a radius r ($0 \le r \le r_1$) excited by a single transmitter with a TRD z in such a multi-cylindrically layer geometry can be written as [19]

$$H(\omega, d, \mathbf{z}, r) = \frac{N_T I r_1}{\pi} \int_0^\infty f(\omega, d, r, \lambda) \cos(\lambda \mathbf{z}) d\lambda \quad (1)$$

where I denotes the transmitting current value, $f(\omega, d, r, \lambda) = xQI_0(xr)$, and d denotes the thickness of the metal casings. Q denotes the reflection coefficient related to the geometrical and electrical parameters of all the layers, and I_0 is a modified Bessel function of the first kind of order zero. In case multiple transmitters are utilized, (1) can be rewritten as:

$$H(\mathbf{I}, \omega, d, \mathbf{z}, r) = \sum_{n=1}^{N} I_n \frac{N_T r_1}{\pi} \int_0^\infty f(\omega, d, r, \lambda) \cos(\lambda \mathbf{z}_n) d\lambda \quad (2)$$

where I_n denotes the nth transmitting current, and $\mathbf{I} = [I_1 I_2 \ldots I_N]^T$. z_n denotes the distance between the receiver and the nth transmitter, and $\mathbf{z} = [z_1 \ z_2 \ \ldots z_N]^T$. In this study, the receiver was located at the center of the transmitter array, so the effect of the symmetry transmitters with the same absolute value of the TRD is the same, as the TRD is included in a cosine function in (1). According to the numerical approximation method in [30], the integration can be expanded as multi-stage Legendre polynomials using the Gauss–Legendre quadrature equation with ($\lambda' + 1$)/2 instead of λ [19]:

$$H(\mathbf{I}, \omega, d, \mathbf{z}, r) = \frac{N_T r_1 \lambda_0}{2\pi} \sum_{n=1}^{N} I_n$$
$$\times \sum_{p=1}^{P} A_p f(\omega, d, r, \lambda_p) \cos(\lambda_p z_n) \quad (3)$$

where $\lambda_p = \lambda_0 (B_p + 1)/2$. P represents the number of stages of the Legendre polynomials, where A and B denote their quadrature coefficient and zero-point, respectively. Considering the monotonically decreasing characteristic of the integrand in (1) with respect to the modified Bessel functions, the upper limit of the infinite integral can be reduced to an approximately limited value of λ_0 ($\lambda_0 = 6000$ in this paper). Then, (3) can be represented using the inner production of three matrixes as follows

$$H(\mathbf{I}, \omega, d, \mathbf{z}, r) = \xi \mathbf{I}^T \mathbf{X}(\mathbf{z}) \mathbf{K}^T(\omega, d, r) \quad (4)$$

where $\xi = (N_T r_1 \lambda_0)/2\pi$

$$\mathbf{X}(\mathbf{z}) = \begin{bmatrix} \mathbf{Y}(z_1) & \mathbf{Y}(z_2) & \cdots & \mathbf{Y}(z_N) \end{bmatrix}^T \in C^{N \times P} \quad (5)$$

$$\mathbf{Y}(z_n) = [\cos(\lambda_1 z_n), \quad \cdots, \quad \cos(\lambda_P z_n)] \in C^{1 \times P} \quad (6)$$

$$\mathbf{K}(\omega, d, r) = [A_1 f(\omega, d, r, \lambda_1), \ldots,$$
$$A_P f(\omega, d, r, \lambda_P)] \in C^{1 \times P} \quad (7)$$

Obviously, from the above equations, it can be concluded that the magnetic field can be focused on using multiple transmitters with different TRDs and transmitting currents. In order to access the MTF effect, we employed the induced electromotive force (EMF) in this study, as the transmit energy is proportional to the induced EMF. The induced EMF of the receiver in the frequency domain can be expressed as:

$$U(\mathbf{I}, \omega, d, \mathbf{z}) = -i\omega\mu_1 N_R \int_0^{r_1} H(\mathbf{I}, \omega, d, \mathbf{z}, r) \cdot 2\pi r dr \quad (8)$$

Given a ramp signal with a turn-off time of t_{of}, the induced EMF in the time domain can be obtained using the Gaver-Stehfest inverse Laplace transform [31] with S stages:

$$U(\mathbf{I}, t, d, z) = \frac{\ln 2}{t} \sum_{s=1}^{S} D_s \frac{e^{(-s \ln 2 t_{of})/t} - 1}{t_{of}(s \ln 2/t)^2} U(\mathbf{I}, s \ln 2/it, d, \mathbf{z}) \quad (9)$$

where it has to be mentioned that suitable stage number ($S = 16$ in this paper) and corresponding filter coefficients have to be selected to reduce the influence of the relative errors of the numerical inversion of the Laplace transform. Then, (9) can be represented in the matrix form as follows

$$U(\mathbf{I}, t, d, \mathbf{z}) = \xi \mathbf{I}^T \mathbf{X}(\mathbf{z}) \mathbf{G}^T(t, d) \quad (10)$$

where

$$\mathbf{G}(t, d) = -\frac{\ln 2 \mu_1 N_R}{t} \sum_{s=1}^{S} D_s \frac{e^{(-s \ln 2 t_{of})/t} - 1}{t_{of}(s \ln 2/t)}$$
$$\times \int_0^{r_1} \mathbf{K}(s \ln 2/it, d, r) \cdot 2\pi r dr \quad (11)$$

According to (10), it can be seen that by changing the currents of the multiple-transmitting array, not only the received signal can be modified to obtain different results but also the magnetic field of the multiple-transmit array. Thus, if the magnetic field can be focused on a certain area at which the receiver is located along the longitudinal axis by weighting the multiple-transmitting array, the magnetic flux of the receiver can be substantially maximized to obtain better SNR and more accurate NDT of downhole casings.

III. MTF FOR THE BOREHOLE TEM SYSTEM

As shown in Section II, the magnetic field distribution as well as the induced EMF can be changed by adjusting the transmitting current value of each transmitter with different TRDs. In [19], the receiving weighting vector were applied to a multiple receiving array and were optimized to improve the detection performance. Correspondingly, the transmitting current of each transmitter plays the same role as the weighting of the multiple-receiving array, and we could also weight the multiple-transmitting current in this study to improve the performance of the borehole TEM system for the NDT of downhole casings. In this section, we demonstrate the LCMV-based MTF for a borehole TEM system with its performance analyses of the SNR.

A. MTF FOR A BOREHOLE TEM SYSTEM

Considering the system noise in the receiver, which is substantially affected by adjusting the transmitting current, we used the term $\mathbf{I}^T\mathbf{N}$ to represent the weighted system noise, where the transmitting current $\mathbf{I}$ was assumed to be a normalized vector without loss of generality. Then, (10) can be rewritten as:

$$U(\mathbf{I}, t, d, \mathbf{z}) = \xi \mathbf{I}^T \mathbf{X}(\mathbf{z})\, G^T(t, d) + \mathbf{I}^T \mathbf{N} \qquad (12)$$

If the transmitting magnetic field range is focused at $z = 0$ ideally, the receiving signal after MTF can be written as $\mathbf{Y}(0)\mathbf{G}^T(t, d)$ which is just the desired part of the received signal of a single transmitter located at $z = 0$, where better SNR can be achieved by using the transmitting array [32]; and the desired signal can be written as:

$$U_d(\mathbf{I}, t, d, \mathbf{z}) = \xi \mathbf{Y}(0)\,\mathbf{G}^T(t, d) \qquad (13)$$

According to the LCMV criterion-based digital beamforming method, we optimized the transmitting currents to obtain the MTF by minimizing the variance of the induced EMF of the receiver. Then, the transmit current could be calculated using the following optimization problem with the LCMV criterion as:

$$\min_{\mathbf{I}}\ \mathbf{I}^T \mathbf{R}_{\hat{U}} \mathbf{I}$$
$$s.t\ \ \mathbf{I}^T \mathbf{X}(\mathbf{z}) = \mathbf{Y}(0) \qquad (14)$$

with

$$\begin{aligned}\mathbf{R}_{\hat{U}} &= E\left\{\hat{U}(t, d, \mathbf{z})\hat{U}(t, d, \mathbf{z})^T\right\} \\ &= \mathbf{R}_B + \mathbf{R}_N\end{aligned} \qquad (15)$$

where $\hat{U}(t, d, \mathbf{z}) = \mathbf{B}(t, d, \mathbf{z}) + \mathbf{N}$, $\mathbf{B}(t, d, \mathbf{z}) = \xi\mathbf{X}(\mathbf{z})\mathbf{G}^T(t, d)$, and $\mathbf{R}_B$ and $\mathbf{R}_N$ denote the signal and noise correlation matrix (NCM), respectively, and $\mathbf{R}_B$ can be written as:

$$\mathbf{R}_B = \xi^2 \mathbf{X}(\mathbf{z})\, E\left\{\mathbf{G}^T(t, d)\, \mathbf{G}(t, d)\right\} \mathbf{X}^T(\mathbf{z}) \qquad (16)$$

Using the Lagrange multiplier method [28], the upper optimization problem can be transformed by introducing the Lagrange operator vector $\boldsymbol{\beta} \in {}^{1 \times P}$, such that

$$\Xi = \mathbf{I}^T \mathbf{R}_{\hat{U}} \mathbf{I} + \boldsymbol{\beta}\left(\mathbf{X}^T(z)\mathbf{I} - \mathbf{Y}(0)^T\right) \qquad (17)$$

where each element of $\boldsymbol{\beta}$ satisfies $0 < \beta_p < 1$, and the optimal weight is:

$$\mathbf{I}_{\text{LCMV}} = \mathbf{R}_{\hat{U}}^{-1}\mathbf{X}(\mathbf{z})\left(\mathbf{X}(\mathbf{z})^T\mathbf{R}_{\hat{U}}^{-1}\mathbf{X}(\mathbf{z})\right)^{-1}\mathbf{Y}(0)^T \qquad (18)$$

Note that, considering the symmetry effect of the TRD on the TEM signal as illustrated in Section II, the number of independent weights should actually be only $\lceil N/2 \rceil$. In this study, the MTF could not only eliminate the influence of the TRDs such as in [19], but it also had an obvious focusing effect. To further analyze the MTF, we discussed the MTF performance in detail.

B. MODIFIED LCMV-BASED MTF

In Section III.A, we showed the LCMV-based multiple-transmit current weighting, where the response of the whole array could be equalized to that of a single transmit with a localization of $z = 0$ so that the focusing could be realized with minimum variance. To make comprehensive performance analyses, we employed the maximum SNR criterion to investigate the transmitting current weight. The SNR of the borehole TEM array response can be expressed as:

$$\text{SNR} = \frac{\mathbf{I}^T \mathbf{R}_B \mathbf{I}}{\mathbf{I}^T \mathbf{R}_N \mathbf{I}} \qquad (19)$$

Assuming that the NCM can be decomposed as $\mathbf{R}_N = \boldsymbol{\Gamma}^T \boldsymbol{\Gamma}$, where $\boldsymbol{\Gamma}$ is invertible, (19) can then be rewritten as:

$$\begin{aligned}&\text{SNR} \\ &= \xi^2 \frac{(\boldsymbol{\Gamma}\mathbf{I})^T\, \boldsymbol{\Gamma}^{-T}\mathbf{X}(\mathbf{z})\, \mathbf{G}^T(t, d)\, \mathbf{G}(t, d)\, \mathbf{X}^T(\mathbf{z})\, \boldsymbol{\Gamma}^{-1}\, (\boldsymbol{\Gamma}\mathbf{I})}{\mathbf{I}^T\boldsymbol{\Gamma}^T\boldsymbol{\Gamma}\mathbf{I}}\end{aligned} \qquad (20)$$

According to the Schwartz inequality $\mathbf{CF}^T\mathbf{FC}^T \leq \mathbf{CC}^T\mathbf{FF}^T$, if is held in the case of $|\mathbf{CF}^T|^2 \leq \mathbf{CC}^T \cdot \mathbf{FF}^T$, let $(\boldsymbol{\Gamma}\mathbf{I})^T = \mathbf{C}$ and $(\boldsymbol{\Gamma}^{-1})^T\mathbf{X}(\mathbf{z})\mathbf{G}^T(t, d) = \mathbf{F}^T$. Then,

$$\begin{aligned}&(\boldsymbol{\Gamma}\mathbf{I})^T\, \boldsymbol{\Gamma}^{-T}\mathbf{X}(\mathbf{z})\, \mathbf{G}^T(t, d)\, \mathbf{G}(t, d)\, \mathbf{X}^T(\mathbf{z})\, \boldsymbol{\Gamma}^{-1}\, (\boldsymbol{\Gamma}\mathbf{I}) \\ &\quad \leq (\boldsymbol{\Gamma}\mathbf{I})^T\, (\boldsymbol{\Gamma}\mathbf{I}) \left(\mathbf{G}(t, d)\, \mathbf{X}^T(\mathbf{z})\, \boldsymbol{\Gamma}^{-1}\right) \\ &\quad\quad \times \left(\mathbf{G}(t, d)\, \mathbf{X}^T(\mathbf{z})\, \boldsymbol{\Gamma}^{-1}\right)^T\end{aligned} \qquad (21)$$

When $\mathbf{C}$ and $\mathbf{F}$ are of the same order and $\mathbf{C} = \chi\mathbf{F}$, the equation is held. Then,

$$\boldsymbol{\Gamma}\mathbf{I} = \chi\left(\boldsymbol{\Gamma}^{-1}\right)^T \mathbf{X}(\mathbf{z})\,\mathbf{G}^T(t, d) \qquad (22)$$

where χ is a single variable, and the solution of (23) becomes

$$\mathbf{I}_{\text{SNR}} = \chi\mathbf{R}_N^{-1}\mathbf{X}(\mathbf{z})\,\mathbf{G}^T(t, d) \qquad (23)$$

It is obvious that the solutions of the transmitting current in (18) and (23) are different, where the LCMV-based optimal weight has a right multiplication vector, while the maximum SNR-based optimal weight only has a single variable as a coefficient. Unfortunately, in [19], an inappropriate conclusion was made which entails that the LCMV-based weight is equivalent to that of the maximum SNR. In this study, we proposed a modified LCMV method by right multiplying the two sides of the subjection condition in (14) by $\mathbf{G}^T(t, d)$, and the LCMV-based multiple-transmitting weighting could be modified as:

$$\min_{\mathbf{I}}\ \mathbf{I}^T \mathbf{R}_{\hat{U}} \mathbf{I}$$
$$s.t\ \ \mathbf{I}^T\mathbf{X}(\mathbf{z})\mathbf{G}^T(t, d) = \mathbf{Y}(0)\,\mathbf{G}^T(t, d) \qquad (24)$$

Note that the right multiplication of $\mathbf{G}^T(t, d)$ does not change the fundamental purpose of the MTF showed in Section III.A, and the optimal solution of (24) can be calculated as follows:

$$\mathbf{I}_{\text{LCMV-M}} = \eta\mathbf{R}_{\hat{U}}^{-1}\mathbf{X}(\mathbf{z})\mathbf{G}^T(t, d) \qquad (25)$$

where $\eta = [\mathbf{G}(t,d)\mathbf{X}^{\mathrm{T}}(\mathbf{z})\mathbf{R}_{\tilde{U}}^{-1}\mathbf{X}(\mathbf{z})\mathbf{G}^{\mathrm{T}}(t,d)]^{-1}\mathbf{Y}(0)\mathbf{G}^{\mathrm{T}}(t,d)$ is a single variable. Similarly, according to the matrix inversion lemma [19], the above weight can be expressed as:

$$\mathbf{I}_{\text{LCMV-M}} = \eta'\mathbf{R}_{\mathrm{N}}^{-1}\mathbf{X}(\mathbf{z})\mathbf{G}^{\mathrm{T}}(t,d) \qquad (26)$$

where η' is a single variable. By comparing (23) and (26), we could find that the modified LCMV-based MTF became equivalent to the maximum SNR criterion-based MTF, meaning that the maximum SNR can be achieved using the modified LCMV method and that the conclusion of [19] is still correct. Notably, in the derivation above, although $\mathbf{G}^{\mathrm{T}}(t,d)$ was unknown, it was not used directly. As an alternative, $\mathbf{XzG}^{\mathrm{T}}(t,d)$ was involved in (12) and could be obtained from the receiving signal. Therefore, the modification of the LCMV subjection did not influence the realization of the MTF method. Moreover, we found that the former weight in section III.A as well as in [19] seems like an ordinary weight that is not correlated to the measured information of the downhole casings. In contrast, using the modified LCMV method, the optimal weight became an adaptive weight for the borehole TEM system.

IV. SUBARRAY PARTITION FOR THE MTF

In Section III, we demonstrated the LCMV-based multiple-transmit focusing method for the NDT of downhole casings using borehole TEM systems, where the maximum SNR could be achieved using the focusing effect, as the combination of all the transmitters could be weighted to be subjected to the transmitter with $z = 0$. In [19], it was shown that better resolutions can be achieved with more weighted elements in the case of the absence of array errors. However, since each transmitter requires a dependent transmit circuit (an H-bridge circuit) for the bipolar TEM transmit, a large number of transmitters was too complex to be realized in downhole detection.

To make multiple transmitting focusing more applicable, we divided the N transmitter into L subarrays, where each subarray used the same transmitting weight, meaning that all the transmitters in each subarray shared one transmitting circuits. The subarray partition structure of the multiple-transmitting array with 9 transmitters divided into 5 subarrays is shown in Fig. 2.

So, under this configuration, the transmitting weights can be rewritten as:

$$\mathbf{I} = \begin{bmatrix} I_{S1} & \cdots & I_{S1} & I_{S2} & \cdots & I_{S2} & \cdots & \cdots & I_{SL} & \cdots & I_{SL} \end{bmatrix}_{N \times 1}^{\mathrm{T}} \qquad (27)$$

where I_{sl} denotes the transmitting current of the transmitter in the lth subarray, and L denotes the number of subarrays. Considering the physical limitations of borehole measurements, the transmitting array can only be larger in the longitudinal direction, which substantially increases the transmitting array length. Also, when an array is too large, some of the transmitters are too far away from the focusing area to have a sufficient effect on the MTF. Therefore, without loss of
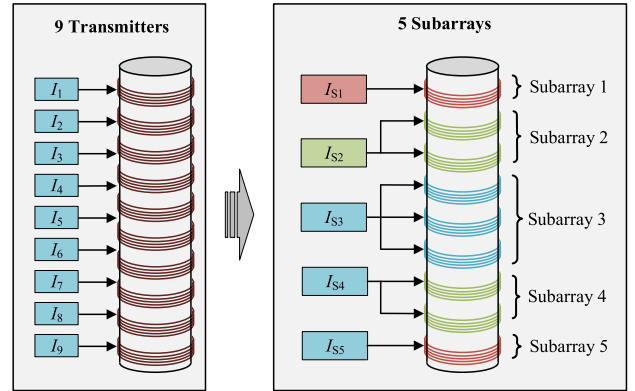

FIGURE 2. Subarray partition structure of the linear multiple-transmitting array.

generality, we assumed that the length of the transmit array is fixed, so the optimal transmitter array was designed using the subarray partition approach. Then, the weight vector can be rewritten as:

$$\mathbf{I}^{\mathrm{T}} = \mathbf{I}_{\mathrm{S}}^{\mathrm{T}}\mathbf{V} \qquad (28)$$

with

$$\mathbf{I}_{\mathrm{S}} = \begin{bmatrix} I_{S1} & I_{S2} & \cdots & I_{SL} \end{bmatrix}_{L \times 1}^{\mathrm{T}} \qquad (29)$$

$$\mathbf{V} = \begin{bmatrix} \overbrace{1 \ \cdots \ 1}^{w_1} & 0 \ \cdots \ 0 & \cdots & 0 \ \cdots \ 0 \\ 0 \ \cdots \ 0 & \underbrace{1 \ \cdots \ 1}_{w_2} & \cdots & 0 \ \cdots \ 0 \\ \vdots & \vdots & \ddots & \vdots \\ 0 \ \cdots \ 0 & 0 \ \cdots \ 0 & \cdots & \underbrace{1 \ \cdots \ 1}_{w_L} \end{bmatrix}_{L \times N} \qquad (30)$$

where w_l denotes the number of transmitters in the lth subarray. By substituting (28) into (12), (12) can be rewritten as:

$$U(\mathbf{I}_{\mathrm{S}}, \mathbf{V}, t, d, \mathbf{z}) = \mathbf{I}_{\mathrm{S}}^{\mathrm{T}}\mathbf{V}\mathbf{B}(t,d,\mathbf{z}) + \mathbf{I}_{\mathrm{S}}^{\mathrm{T}}\mathbf{V}\mathbf{N} \qquad (31)$$

By substituting (28) into (24), the LCMV criterion can be rewritten as:

$$\min_{\mathbf{I}_{\mathrm{S}}} \ \mathbf{I}_{\mathrm{S}}^{\mathrm{T}}\mathbf{R}_{\mathrm{VU}}\mathbf{I}_{\mathrm{S}}$$
$$s.t \ \ \mathbf{I}_{\mathrm{S}}^{\mathrm{T}}\mathbf{V}\mathbf{X}(\mathbf{z})\mathbf{G}^{\mathrm{T}}(t,d) = \mathbf{Y}(0)\mathbf{G}^{\mathrm{T}}(t,d) \qquad (32)$$

where $\mathbf{R}_{\mathrm{VU}}$ denotes the auto-correlation matrix and can be calculated as:

$$\mathbf{R}_{\mathrm{VU}} = E\left\{ (\mathbf{V}\mathbf{B}(t,d,\mathbf{z}) + \mathbf{V}\mathbf{N})(\mathbf{V}\mathbf{B}(t,d,\mathbf{z}) + \mathbf{V}\mathbf{N})^{\mathrm{T}} \right\} \qquad (33)$$

Using the Lagrange multiplier method in Section III, the optimal weight for the subarray partition can be given by:

$$\mathbf{I}_{\text{S-LCMV}} = \kappa\mathbf{R}_{\mathrm{VU}}^{-1}\mathbf{X}(\mathbf{z})\mathbf{G}^{\mathrm{T}}(t,d) \qquad (34)$$

where κ is a single variable. It is substantial that the subarray partition approach can significantly reduce the MTF complexity; however, the performance loss would be unavoidable. Since different subarray partitions can result in different focusing performances, the subarray partition selection needs to be designed with a small number of independent weights with the least possible performance loss. In this study, we used the MSE as standard for the subarray selection:

$$\text{MSE} = E\left\{U(\mathbf{I}_{\text{S-LCMV}}, \mathbf{V}, t, d, \mathbf{z}) - U_d(\mathbf{I}_{\text{S-LCMV}}^{\text{T}}\mathbf{V}, t, d, \mathbf{z})\right\}$$
(35)

Although the MSE criterion is equal to the LCMV criterion for multiple-transmit borehole TEM arrays, the MSE is substantially decreased due to the reduced dimension of the subarray partition. Unfortunately, the optimization problem of (35) involves two variables of the number of subarrays and the partition ways, which makes it very difficult to be solved. In order to find an approximate solution, we had to go through all the possible selections to find the minimum MSE regulation.

V. FIELD EXPERIMENTS

The validity of the proposed borehole TEM system was confirmed using field experiments. A standard $5^{1/2}$ inch casing with a thickness of 9.17 mm, thickness decreases of 1.5 mm, 1.7 mm, and 2 mm, and widths of 100 mm, 100 mm, and 125 mm, respectively, were utilized for the NDT. Moreover, to make the MTF effect clear, we used a symmetry array with 9 transmitters, where the fifth transmitter and the receiver were set at the center of the array with $z = 0$. Note that motion measurement of the experimental sensor is required to go through the whole casing. The parameters of the transmit array and receiver are shown in Table 1. The experiment structure of the motion measurements with above experimental setup is shown in Fig. 3 as follows.

TABLE 1. Parameters of the multiple-transmit sensors and field experiment.

Parameter	Symbol	Value
Radius of the multiple transmitters	r_1	12 mm
Number of the transmitters	N	9
Inter-element spacing	Δz	30 mm
Number of receiving coil turns	N_R	166
Number of transmitting coil turns	N_T	62
Wire diameter of the receiving coils	d_R	0.18 mm
Wire diameter of the transmitting coils	d_T	0.24 mm
Length of transmitting array	l_A	255 mm
Length of the transmitters	l_T	15 mm

As shown in Fig. 4 and 5, by using nine transmitting structural sensors to move longitudinally through the casing, we compared three typical kinds of cases of the transmitting schemes. In the first case, we only employed one of the nine transmitters with a transmitting current of 1, and all the other transmitters were closed for emitting with a transmitting current of 0 (termed as Transmitter 1 to 9). In the second case, all the nine transmitters were open for
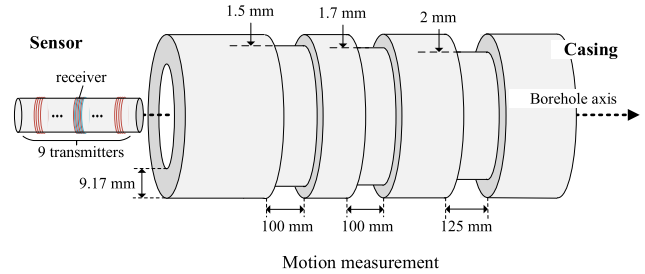
emitting at the same time without transmit weighting (termed as Unweighted array). As an alternative, the third case used the proposed MTF method for all the nine transmitters that were weighted for emitting simultaneously (termed as the MTF with 9 subarrays). Note that the transmitting current vector $\mathbf{I}$ for all the cases was normalized without loss of generality. The normalized induced EMFs of the nine single transmitters are shown in Fig. 4. The casing thicknesses, the EMFs of Transmitter 5, the Unweighted transmitting, and the MTF were compared, as shown in Fig. 5, using 9 subarrays.
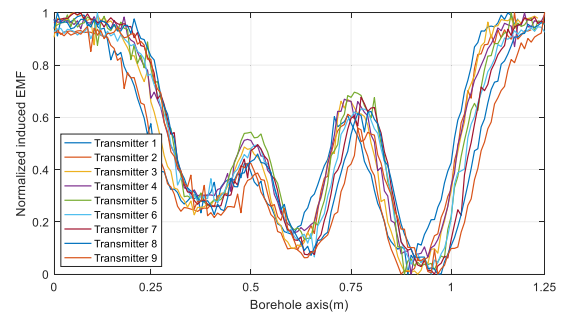

FIGURE 3. The experiment structure of the motion measurements with 9 transmitters and 1 receiver for the NDT of a standard $5^{1/2}$ inch casing with a thickness of 9.17 mm, thickness decreases of 1.5 mm, 1.7 mm, and 2 mm, and widths of 100 mm, 100 mm, and 125 mm, respectively.

FIGURE 4. Normalized induced electromagnetic forces (EMFs) of the receiver with the 9 transmitters open for emitting.
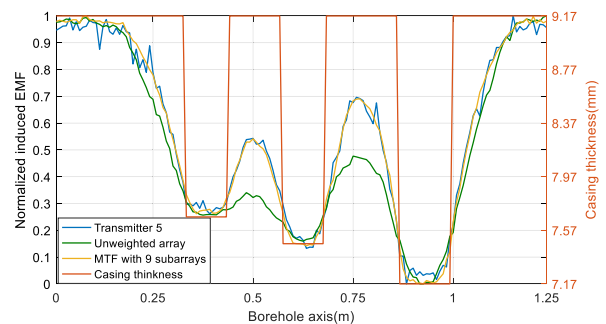

FIGURE 5. Casing thicknesses and the EMFs of the receiver only Transmitter 5 open for emitting; All the 9 transmitters were open for emitting at the same time with and without multiple-transmit focusing (MTF).

The three negative peaks of the EMF curves in Fig. 4 and 5 correspond to the decreases in the thickness in Fig. 5 with different levels and widths. From Fig. 4, it can be observed that the differences in the induced EMF of different transmitters

is mainly manifested as phase 'shifting' in the longitudinal direction. Thus, if all the nine transmitters were simultaneously utilized for emitting without weighting in the second case, it would be equal to a linear accumulation of the nine EMF curves in Fig. 4, and the shifting and distortion would have a great influence on the NDT performance of the metal casings. Obviously, in Fig. 5, it can be seen that the three negative peaks of unweighted array EMF curve is difficult to distinguish in comparison with the MTF and the Transmitter 5 cases, so a high longitudinal resolution can be achieved using the proposed MTF method. Moreover, the induced EMF curve of the MTF case was smoother than that of the Transmitter 5 case, as the SNR of the MTF was maximized. Although the proposed MTF method performed better than both the traditional single transmitter and the unweighted multiple transmitters, implementing the MTF with too many independent transmitters is too complex to realize since each independent transmitter requires an independent transmit circuit. In Section IV, we proposed a subarray partition method to simplify the MTF implementation with fewer independent weights. In the next section, we show the experimental results using the subarray partition approach.

Taking the three total subarrays as an example, the nine transmitting elements could be divided into three subarrays, and the received EMFs in different subarray partition ways were compared, as shown in Fig. 6. To compare the performance of different partition schemes, we assumed the three subarrays to be termed as Subarray A, B, and C, respectively, where subarrays A and C are symmetrical. Then, there were four types of subarray combinations, including Scheme 1 (A: transmitter 1, B: transmitters 2–8, C: transmitter 9), Scheme 2 (A: transmitters 1–2, B: transmitters 3–7, C: transmitters 8–9), Scheme 3 (A: transmitters 1–3, B: transmitters 4–6, C: transmitters 7–9), and Scheme 4 (A: transmitters 1–4, B: transmitter 5, C: transmitters 6–9). Fig. 6 shows the induced EMFs using different partition schemes of the multiple transmitters. We could find that different partition methods have different performances in regards to distinguishing the three negative peaks with respect to the decreases in the thickness. Even though the results could not reach the level of the MTF with the 9 subarrays, all the three subarray schemes could improve the longitudinal performance in comparison with the unweighted transmitting method. In the next section, we show the influence of the number of independent weights in regards to the subarray partitions.

Fig. 7 compares the induced EMFs of the subarray partition method with different numbers of subarrays, where the chosen partition schemes for each case correspond to the best MSE performance that can be achieved with a limited number of subarrays. From Fig. 7, it can be seen that with the increase in the subarray numbers, the focusing performance also correspondingly increased. Thus, obviously, using a small number of subarrays makes the MTF easier to implement but also leads to a performance loss in the longitudinal resolution. As a result, the subarray partition selection can be a considerable method to make a trade-off design between the hardware
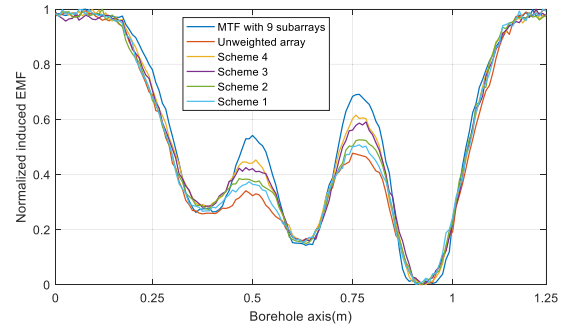

FIGURE 6. Comparison of the induced EMFs between the 9 transmitters that were opened for emitting simultaneously with and without MTF weighting and the MTF array with 3 subarrays using different partition schemes.
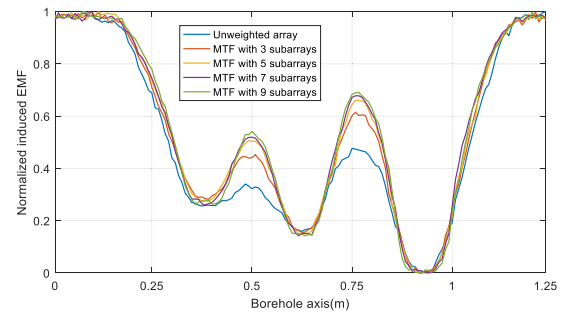

FIGURE 7. Comparison of the induced EMFs between the 9 transmitters that were opened for emitting simultaneously with and without MTF weighting and the MTF array with the subarray numbers of 3, 5, and 7.
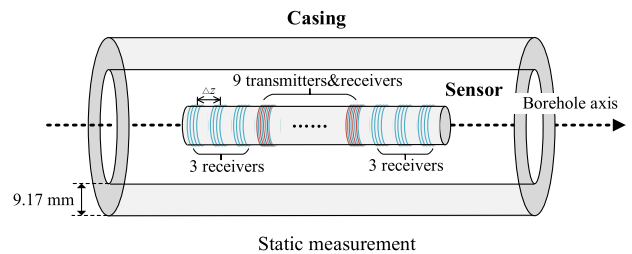

FIGURE 8. The experiment structure of the static measurements using sensor structures with 9 transmitters and 15 receivers with an inter-element spacing of Δz for the NDT of a standard $5^{1/2}$ inch undamaged casing with a thickness of 9.17 mm.

implementation and longitudinal resolution. To further investigate the focusing performance, we set 15 receivers along the borehole axis to access the MTF effect statically by evaluating the distribution of the transmit magnetic fields in an undamaged casing as shown in Fig. 8.

On the basis of the static measurement of the casing with the above 9 transmitting and 15 receiving structures, Fig. 9 compares the magnetic focusing effect of the proposed MTF method on the induced EMFs with different subarray partition schemes, where the subarray numbers were set to 1, 3, 5, 7, and 9, respectively. The first case with only one subarray was equal to the unweighted array, as shown in Fig. 5. In the other cases, the chosen partition schemes for each case corresponded to the best MSE performance, as shown in Section IV. Fig. 9 (a) (b) show the EMFs of the 15 receivers

for the NDT of the metal casing with a thickness of 9.17 mm (standard specification of $5^{1/2}$ inch casing) at sampling times of 20 ms and 50 ms. From Fig. 9, we could observe that the normalized induced EMFs perform like a 'beam' with respect to the transmit energy, where the widths of the beam of the MTF method are more narrowly than that of the unweighted case for both the early and late sampling times, which reveals the magnetic field can be focused more effectively on the center of the transmit array ($z = 0$). As a result, with a narrower focusing beam, the magnetic flux of the receive coil with the certain longitudinal position will be substantially concentrated to obtain better SNR, and the induced EMFs will be more accurate as it contains more information related to that area. Specifically, the earlier magnetic field performed better in the longitudinal resolution compared with the latter one because of the diffusion property of the TEM techniques. Moreover, it is obvious that the focusing effect as well as the longitudinal resolution were proportional to the number of subarrays.
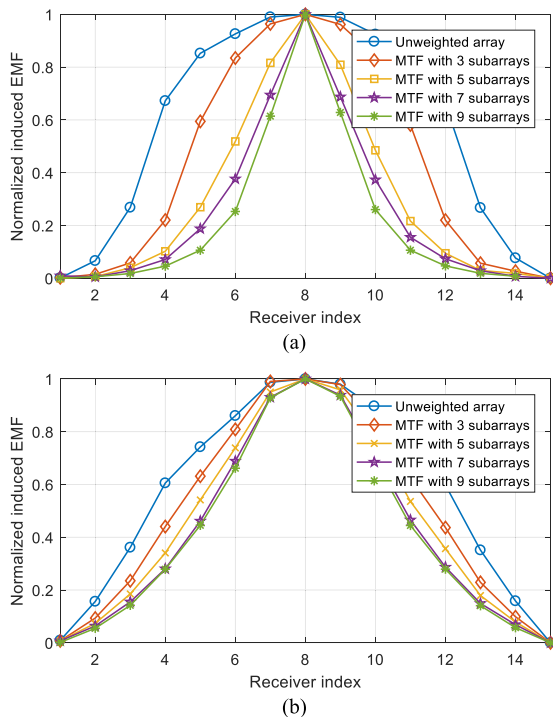

FIGURE 9. Comparison of the induced EMFs of the 15 receivers between the unweighted array and MTF array with different numbers of subarrays at the sample times of (a) 20 ms and (b) 50 ms.

Without a loss in generality, the simulations of the comparison using the MSE defined in Section IV to illustrate the effect of the number of independent weights was conducted. Fig. 10 shows the normalized MSE versus the number of subarrays using the subarray schemes with the uniform partition and minimum MSE partitions, respectively, where the number of transmitting array elements was set to 120, the inter-element space was 0.5 cm, and the receiver was located at the middle of the transmitting array. The transmitting array

elements could be divided into one subarray at least, where the transmitting elements were emitted at the same time without weighting, and 120 subarrays at most, where each element of the transmitting arrays was regarded as one subarray. In the uniform partition scheme, each subarray had the same number of transmitting elements. In contrast, the minimum MSE partition scheme corresponded to the best MSE performance and was usually not the uniform partition scheme. It can be seen from Fig. 10 that the MSE performance of the subarray partition-based MTF is inversely proportional to the number of subarrays and that the best performance can be obtained when the number of subarrays is maximized to 120.
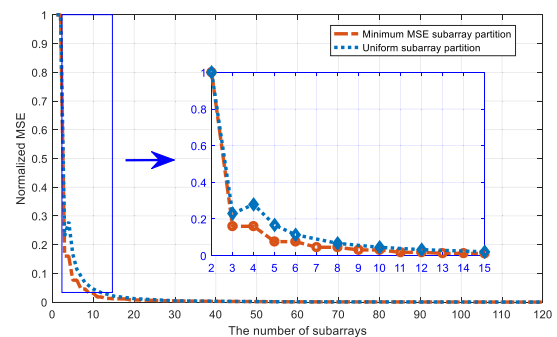

FIGURE 10. Comparison of the normalized MSE between the uniform subarray partition and the minimum MSE subarray partition versus the number of subarrays.

Notably, since the TEM model is centrosymmetric, the weighting and subarray partition methods are also symmetrical at the middle of the transmitting array. Therefore, when the transmitting array was divided into $2L$ subarrays with the minimum MSE partition scheme, the number of array elements and the weighting coefficient of the two center subarrays (the Lth and $L + 1$th subarrays) were the same due to the symmetrical characteristic of the transmitting array so that they can be equivalent to one subarray, and the MSE performance of the $2L$ subarrays and $2L$-1 subarrays was also the same. By comparing the two curves in Fig. 10, although the MSE curves were all monotonically decreased with the number of subarrays, in most cases, the uniform partition should not be the best scheme to achieve minimum MSE with the same number of subarrays, and the fast search of the minimum MSE scheme would be an interesting problem to be investigated.

VI. CONCLUSION
In this study, an MTF-based borehole TEM system was proposed to improve the NDT performance for downhole casings. We derived the response of the multiple-transmit array into the matrix form, and the results showed that the excited magnetic field using the multiple-transmit array can be focused by weighting the current of each transmitter. Using this property, a modified LCMV-based multiple-transmitting array weighting method was presented to realize magnetic focusing. Moreover, a subarray partition approach was proposed to simplify the MTF realization, where the subarray

weighting and the MSE were also analyzed. The simulation and experiment results demonstrated the effectiveness of the proposed system.

REFERENCES

[1] L. Tusa, L. Andreani, M. Khodadadzadeh, C. Contreras, P. Ivascanu, R. Gloaguen, and J. Gutzmer, "Mineral mapping and vein detection in hyperspectral drill-core scans: Application to porphyry-type mineralization," *Minerals*, vol. 9, no. 122, pp. 1–23, Feb. 2019.

[2] J. Cheng, J. Xue, J. Zhou, Y. Dong, and L. Wen, "2.5-D inversion of advanced detection transient electromagnetic method in full space," *IEEE Access*, vol. 8, pp. 4972–4979, 2020.

[3] J. Li, Z. He, and N. Feng, "Preconditioned inversion of 3D borehole to surface electromagnetic for reservoir exploration," *Pure Appl. Geophys.*, vol. 176, no. 12, pp. 5349–5362, Jul. 2019.

[4] B. Hu, H. Li, X. Zhang, and L. Fang, "Oil and gas mining deformation monitoring and assessments of disaster: Using interferometric synthetic aperture radar technology," *IEEE Geosci. Remote Sens. Mag.*, vol. 8, no. 2, pp. 108–134, Jun. 2020.

[5] S.-M. Hsu, C. C. Ke, Y. T. Lin, C. C. Huang, and Y. S. Wang, "Unravelling preferential flow paths and estimating groundwater potential in a fractured metamorphic aquifer in taiwan by using borehole logs and hybrid DFN/EPM model," *Environ. Earth Sci.*, vol. 78, no. 5, pp. 1–22, Feb. 2019.

[6] L. Zhao, C.-J. Li, Z.-X. Duan, W. Wang, and X.-D. Wu, "The metal thickness detection using pulsed eddy-current computation and detection method," *Cluster Comput.*, vol. 22, no. S3, pp. 6551–6562, May 2019.

[7] B. Dang, L. Yang, R. Dang, and Y. Xie, "Borehole electromagnetic induction system with noise cancelation for casing inspection," *IEICE Electron Express*, vol. 13, no. 17, pp. 1–9, Jul. 2016.

[8] X. Chen and J. Li, "Pulsed eddy current testing for electromagnetic parameters of a spherical conductor," *IEEE Sensors J.*, vol. 20, no. 7, pp. 3627–3635, Apr. 2020.

[9] A. I. Mohammed, B. F. Oyeneyin, B. Atchisonb, and J. Njuguna, "Casing structural integrity and failure modes in a range of well types-A review," *J. Natural Gas Sci. Eng.*, vol. 68, pp. 1–9, Jun. 2019.

[10] F. Selker and J. Selker, "Investigating water movement within and near wells using active point heating and fiber optic distributed temperature sensing," *Sensors*, vol. 18, no. 4, p. 1023, Mar. 2018.

[11] Y. A. Plotnikov, F. W. Wheeler, S. Mandal, W. R. Ross, J. S. Price, E. J. Nieters, A. Ivan, S. Dolinsky, H. C. Climent, and A. M. Kasten, "Development of an electromagnetic imaging system for well bore integrity inspection," in *Proc. 43rd Annu. Rev. Prog. Quant. Nondestruct. Eval.*, Niskayuna, NY, USA, Feb. 2017, pp. 1–9.

[12] B. Dang, C. Liu, L. Yang, G. Wang, M. Wang, Z. Ren, and R. Dang, "EMD-based borehole TEM array signal denoising and baseline wander correction for NDT of downhole casings," *IEEE Access*, vol. 8, pp. 150213–150224, 2020.

[13] W. Chen, S. Han, M. Y. Khan, W. Chen, Y. He, L. Zhang, D. Hou, and G. Xue, "A Surface-to-Borehole TEM system based on grounded-wire sources: Synthetic modeling and data inversion," *Pure Appl. Geophys.*, vol. 177, no. 9, pp. 4207–4216, Apr. 2020.

[14] T. Wu, J. R. Bowler, and T. P. Theodoulidis, "Eddy-current induction by a coil whose axis is perpendicular to that of a tube," *IEEE Trans. Magn.*, vol. 53, no. 7, pp. 1–9, Jul. 2017.

[15] Y. Fu, R. Yu, X. Peng, and S. Ren, "Investigation of casing inspection through tubing with pulsed eddy current," *Nondestruct. Test. Eval.*, vol. 27, no. 4, pp. 353–374, Dec. 2012.

[16] Q. Luo, Y. Shi, Z. Wang, W. Zhang, and D. Ma, "Method for removing secondary peaks in remote field eddy current testing of pipes," *J. Nondestruct. Eval.*, vol. 36, no. 1, pp. 1–11, Mar. 2017.

[17] C. Yang, B. Gao, Q. Ma, L. Xie, G. Y. Tian, and Y. Yin, "Multi-layer magnetic focusing sensor structure for pulsed remote field eddy current," *IEEE Sensors J.*, vol. 19, no. 7, pp. 2490–2499, Apr. 2019.

[18] R. Falque, T. Vidal-Calleja, and J. Miro, "Defect detection and segmentation framework for remote field eddy current sensor data," *Sensors*, vol. 17, no. 10, p. 2276, Oct. 2017.

[19] B. Dang, L. Yang, C. Z. Liu, Y. H. Zheng, H. Li, R. Dang, and B. Q. Sun, "A uniform linear multi-coil array-based borehole transient electromagnetic system for non-destructive evaluations of downhole casings," *Sensors*, vol. 18, no. 8, pp. 1–16, Aug. 2018.

[20] N. Zhang, S. Wang, S. Ning, and S. Wang, "Study on planar coil with multi-frequency stimulations applied to an eddy current non-destructive testing," in *Proc. 20th Int. Conf. Electr. Mach. Syst. (ICEMS)*, Aug. 2017, pp. 1–4.

[21] O. Postolache, A. L. Ribeiro, and H. Ramos, "A novel uniform eddy current probe with GMR for nondestructive testing applications," in *Proc. IEEE EUROCON - Int. Conf. Comput. Tool*, Apr. 2011, pp. 1–4.

[22] N. Tsopelas, J. Sarris, and N. J. Siakavellas, "The influence of the exciting frequency on crack detection by eddy current thermography," *Nondestruct. Test. Eval.*, vol. 28, no. 3, pp. 263–277, Sep. 2013.

[23] D. Rifai, A. Abdalla, R. Razali, K. Ali, and M. Faraj, "An eddy current testing platform system for pipe defect inspection based on an optimized eddy current technique probe design," *Sensors*, vol. 17, no. 3, p. 579, Mar. 2017.

[24] H. T. Zhou, K. Hou, H. L. Pan, J. J. Chen, and Q. M. Wang, "Study on the optimization of eddy current testing coil and the defect detection sensitivity," *Procedia Eng.*, vol. 130, pp. 1649–1657, Jan. 2015.

[25] B. L. N. C. Dang Yang Du and R. B. Y. Liu Dang Wang Xie, "Auxiliary sensor-based borehole transient electromagnetic system for the nondestructive inspection of multipipe strings," *Sensors*, vol. 17, no. 8, pp. 1–15, Aug. 2017.

[26] B. H. Choi, J. H. Kim, J. P. Cheon, and C. T. Rim, "Synthesized magnetic field focusing using a current-controlled coil array," *IEEE Magn. Lett.*, vol. 7, pp. 1–4, Jan. 2016.

[27] Q. Meng, X. Hu, H. Pan, and Y. Xi, "Apparent resistivity for transient electromagnetic induction logging and its correction in radial layer identification," *J. Appl. Geophys.*, vol. 151, pp. 328–342, Apr. 2018.

[28] J. Shiriyev, Y. Brick, P. Zhang, A. E. Yilmaz, C. Torres-Verdín, M. M. Sharma, T. Hosbach, M. A. Oerkfitz, and J. Gabelmann, "Experiments and simulations of a prototype triaxial electromagnetic induction logging tool for open-hole hydraulic fracture diagnostics," *Geophysics*, vol. 83, no. 3, pp. D73–D81, May 2018.

[29] A. El-Keyi and B. Champagne, "Adaptive linearly constrained minimum variance beamforming for multiuser cooperative relaying using the Kalman filter," *IEEE Trans. Wireless Commun.*, vol. 9, no. 2, pp. 641–651, Feb. 2010.

[30] P. N. Swarztrauber, "On computing the points and weights for gauss-legendre quadrature," *SIAM J. Sci. Comput.*, vol. 24, no. 3, pp. 945–954, Jan. 2003.

[31] F. Tossani, F. Napolitano, and A. Borghetti, "Inverse laplace transform of the ground impedance matrix of overhead lines," *IEEE Trans. Electromagn. Compat.*, vol. 60, no. 6, pp. 2033–2036, Dec. 2018.

[32] X. Liu, T. Huang, Y. Liu, and J. Zhou, "Joint transmit beamforming for multiuser MIMO communication and MIMO radar," in *Proc. IEEE Int. Conf. Signal, Inf. Data Process. (ICSIDP)*, Dec. 2019, pp. 1–6.
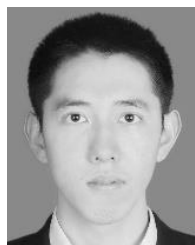
CHANGZAN LIU was born in Hebei, China, in 1989. He is currently pursuing the Ph.D. degree in information and communication engineering from Northwestern Polytechnical University, Xi'an, China. His research interest includes downhole transient electromagnetic system for reservoir exploration.

BO DANG was born in Xi'an, China, in 1987. He received the Ph.D. degree in signal and information processing from Xidian University, in 2013. Since 2014, he has been with the Department of Electronic Engineering, Xi'an Shiyou University. He is currently an Assistant Professor with the Department of Electronic Engineering. His research interest includes downhole transient electromagnetic system for nondestructive testing and evaluation of casing and tubing.

HAIYAN WANG (Member, IEEE) received the B.S., M.S., and Ph.D. degrees in electrical engineering from the School of Marine Science and Technology, Northwestern Polytechnical University (NPU), Xi'an, China, in 1987, 1990, and 2004, respectively. He has been a Faculty Member with NPU, since 1990, and a Professor, since 2004. He teaches and conducts research with NPU in the areas of signal and information processing, electronic engineer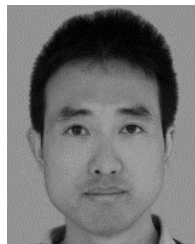ing, and tracking and locating maneuvering targets. His research interests include modern signal processing, array signal processing, underwater acoustic communications, tracking and locating of maneuvering targets, and data mining technique and its application.

XIAOHONG SHEN (Member, IEEE) received the B.S., M.S., and Ph.D. degrees in electrical engineering from Northwestern Polytechnical University (NPU), Xi'an, China, in 1987, 1998, and 2008, respectively. She is currently a Full Professor with the School of Marine Science and Technology, NPU. Her research interests include signal processing, underwater acoustic high data rate communication, underwater acoustic sensor networks, and underwater acoustic communication and networking.
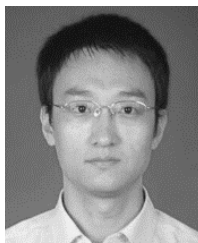
LING YANG was born in Shaanxi, China, in 1993. She is currently pursuing the Ph.D. degree in oil and gas engineering with Xi'an Shiyou University, Xi'an, China. Her research interests include downhole transient electromagnetic oil and gas resource detection.

ZHIPING REN (Member, IEEE) was born in 1980. He received the Ph.D. degree from Chang'an University. He is currently an Associate Professor with the Department of Electronic Engineering, Xi'an Shiyou University, China. His research interests include nondestructive testing and evaluation of downhole casing.

RUIRONG DANG was born in 1957. He received the Ph.D. degree from the Nanjing University of Science and Technology, in 1991. He is currently a Professor with the Shaanxi Key Laboratory of Measurement and Control Technology for Oil and Gas Wells, Xi'an Shiyou University, China. His current research interests include intelligent well layered measurement and control systems.

YUZHU KANG (Graduate Student Member, IEEE) received the M.S. degree in signal and information processing from the School of Information Engineering, Wuhan University of Technology, Wuhan, China, in 2014. He is currently pursuing the Ph.D. degree in information and communication engineering with Northwestern Polytechnical University, Xi'an, China. From 2014 to 2017, he was an Engineer of a technology company in Shenzhen, engaged in computer vision and software development. His current research interests include target localization in underwater acoustic sensor networks and signal processing.

BAOQUAN SUN was born in 1965. He received the B.S. and M.S. degrees in mechanical Engineering from the China University of Petroleum, Dongying, China, in 1987 and 2004, respectively. His current research interests include intelligent oil production measurement and control.

● ● ●